Fast Response, Vertically Oriented Graphene Nanosheet Electric Double Layer Capacitors Synthesized from C_2H_2

Minzhen Cai,[†] Ronald A. Outlaw,[†,*] Ronald A. Quinlan,[†,‡] Dilshan Premathilake,[†] Sue M. Butler,[§] and John R. Miller[§,⊥]

[†]Department of Applied Science, The College of William and Mary, Williamsburg, Virginia 23187, United States, [‡]Materials and Power Systems Branch, Naval Surface Warfare Center, Carderock Division, West Bethesda, Maryland 20817, United States, [§]JME, Inc., 23500 Mercantile Road Suite L, Beachwood, Ohio 44122, United States, and [⊥]Case Western Reserve University, Great Lakes Energy Institute, Cleveland, Ohio 44106, United States

ABSTRACT The growth and electrical characteristics of vertically oriented graphene nanosheets grown by radio frequency plasma-enhanced chemical vapor deposition from C_2H_2 feedstock on nickel substrates and used as electrodes in symmetric electric double layer capacitors (EDLC) are presented. The nanosheets exhibited 2.7 times faster growth rate and much greater specific capacitance for a given growth time than CH_4 synthesized films. Raman spectra showed that the intensity ratio of the D band to G band *versus* temperature initially decreased to a minimum value of 0.45 at a growth temperature of 750 °C, but increased rapidly with further temperature increase (1.15 at 850 °C). The AC specific capacitance at 120 Hz of these EDLC devices increased in a linear fashion with growth temperature, up to 265 μF/cm^2 (2 μm high film, 850 °C with 10 min growth). These devices exhibited ultrafast frequency response: the frequency response at −45° phase angle reached over 20 kHz. Consistent with the increase in D band to G band ratio, the morphology of the films became less vertical, less crystalline, and disordered at substrate temperatures of 800 °C and above. This deterioration in morphology resulted in an increase in graphene surface area and defect density, which, in turn, contributed to the increased capacitance, as well as a slight decrease in frequency response. The low equivalent series resistance varied from 0.07 to 0.08 Ω and was attributed to the significant carbon incorporation into the Ni substrate.

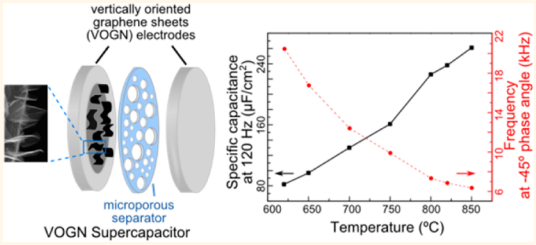

KEYWORDS: graphene · EDLC · electrodes · RF-PECVD · AC filtering · energy storage

Capacitors capable of working at high frequency are in a growing demand.[1] Many applications, such as high-power load leveling, ripple-current filtering, power conversion, and fast pulsed power generation, require capacitors to have quick response in absorbing and releasing energy.[1−3] To date, aluminum electrolytic capacitors are still the primary capacitors used in these applications; however, they are large, bulky and typically fail abruptly, impacting their reliability. The traditional electric double layer capacitors (EDLCs) that are typically based on porous carbon electrodes are considered slow response devices when compared to electrolytic capacitors and cannot meet the filtering requirements. For example, conventional carbon-based EDLCs have an impedance phase angle that is near 0° at 120 Hz, which is far from the −90° value required for ripple-current filtering.[4−6] Substantial efforts have been devoted to developing fast response EDLCs. Carbon nanotube EDLCs achieved an impedance phase angle at 120 Hz of −10° to −65° but were unable to efficiently filter ripples.[7−10] Chemically modified graphene EDLCs show very high capacitance; however, the inherent small pore diameters and long path lengths create unwanted porous electrode behavior that severely limit effective filtering.[11−14] Recently, electrochemically reduced graphite oxide electrodes were reported and exhibited an impedance phase angle of −84° at 120 Hz, however, with limited capacitance.[15] EDLCs made from vertically oriented graphene nanosheet (VOGN) using radio frequency plasma

* Address correspondence to raoutl@wm.edu.

Received for review February 16, 2014 and accepted May 5, 2014.

Published online May 05, 2014
10.1021/nn5009319

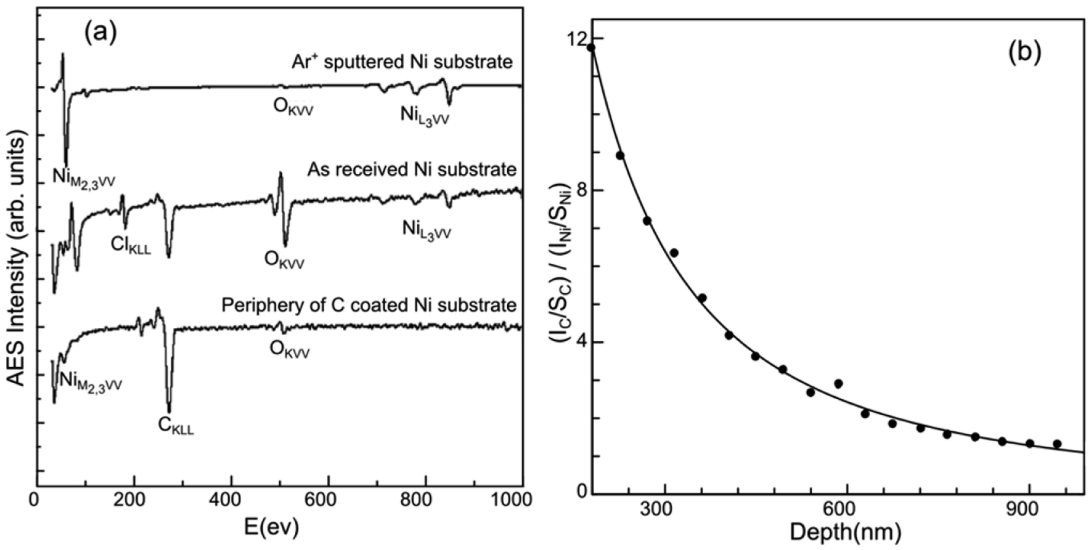

Figure 1. (a) Auger surveys of the Ni substrate sputter cleaned (top) and as received (center), and the mask-covered no-growth periphery Ni outside the center VOGN region (bottom). (b) Depth profile of the C/Ni intensity ratio measured in the no-growth periphery.

enhanced chemical vapor deposition (RF-PECVD) have been studied and show fast response with efficient filtering at 120 Hz.[3,16,17] The open morphology of VOGN provides high conductance channels for ingress and egress of the electrolyte ions between the vertical nanosheets, thus minimizing porous electrode behavior and allowing fast response.

In this paper, the electrical performance of capacitors composed of vertically oriented graphene nanosheets grown from C_2H_2 feedstock on Ni substrates by RF-PECVD was evaluated and compared with similar EDLCs synthesized using CH_4 feedstock. The EDLCs symmetric electrodes were fabricated from VOGN on Ni foil grown over the temperature range of 620−850 °C. All capacitors show excellent frequency response and effective filtering ability. At low temperature, the graphene films exhibit a vertical and ordered geometry which is easy accessible to electrolytic ions. When coupled with the high electron transport of graphene and the negligible contact resistance to the metal current collectors, the resulting EDLCs provide exceptional dynamic response. Although the nanosheets evolved into a more disordered structure at growth temperatures above 800 °C, the accessible surface area and defect density increased, which, in turn, contributed to increased capacitances. This paper reports the research and development of the most advanced, highest-frequency-response electric double layer capacitor ever produced, offering performance comparable to aluminum electrolytic capacitor technology. It will be shown that the use of C_2H_2 feedstock compared to CH_4 feedstock to grow VOGN/Ni EDLCs provides nearly three times faster growth and twice the specific capacitance with virtually no loss in frequency response.

RESULTS

Carbon Diffusion in the Nickel Substrate. Vertically oriented graphene nanosheets were synthesized on Ni substrates using RF-PECVD. During deposition, a tantalum mask was placed on top of the substrates to define the graphene growth region. Figure 1a shows the sputter cleaned Auger electron spectroscopy (AES) survey of the surface (top) which can be compared to the degreased as-received surface with contaminants of C, O, and Cl (center). The bottom AES survey was taken from the periphery of the substrate that was covered by the Ta mask during deposition (so therefore uncoated). However, the predominant signal from the periphery is carbon, not nickel. A slight oxygen signal from re-exposure to the atmosphere was also observed. No segregation of other bulk impurities was observed. This suggests that the substrate temperature during deposition (620−850 °C) was sufficient to cause carbon to dissolve into the bulk and diffuse radially outward from the central deposition region into the uncoated mask-protected periphery. Figure 1b shows the depth profile of the ratio of C_{KLL} to Ni_{MVV} intensities in this uncoated region. The 12 h of Ar^+ sputtering to a depth of ~1 μm could not remove the C signal, but eventually, the ratio approached a constant level associated with C saturation in the Ni bulk. This suggests the carbon species in the plasma adsorbed and then dissolved well into Ni substrates, thus producing ohmic bonding between the VOGN and the substrate. The AES survey of VOGN films shows only the carbon "dolphin peak" at 270 eV with no other elements. X-ray photoelectron spectroscopy was also conducted. Only the C 1s peak was observed. These results indicate that the graphene films are free of contamination (<1%).

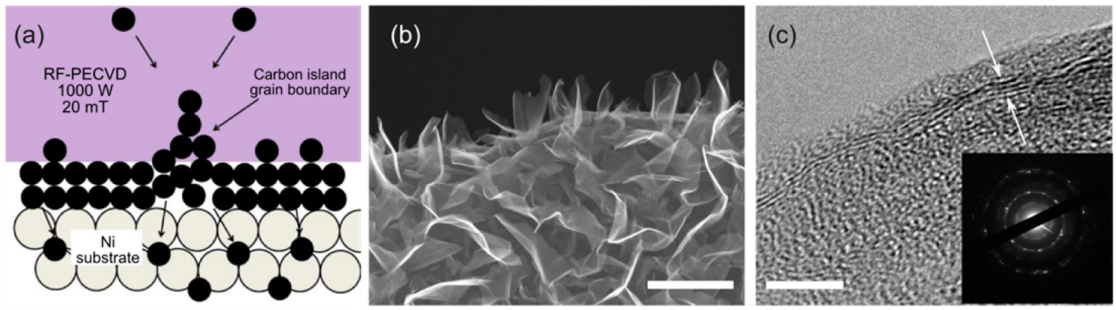

Figure 2. (a) A schematic showing graphite island impingement and upward growth. (b) SEM image of VOGN on a cylindrical grid element from a shallow-angle view. The scale bar is 500 nm. (c) TEM of typical edges of VOGN sheet showing four graphene sheets. Inset is selected area diffraction pattern of VOGN wall. The scale bar is 5 nm.

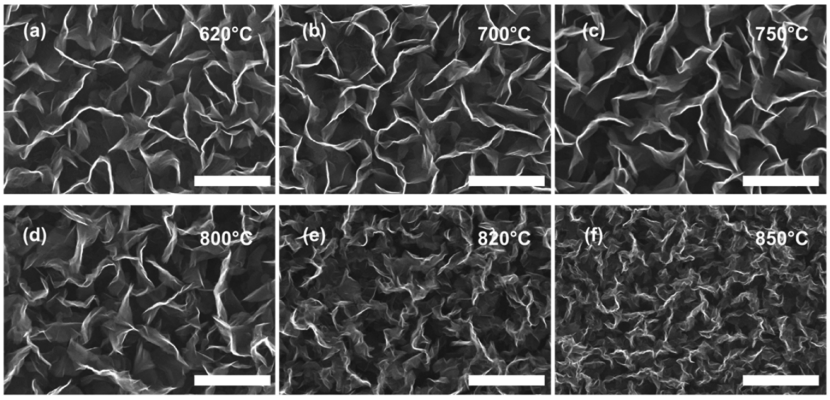

Figure 3. Morphology (plan view) of the VOGN films as a function of deposition temperature. The verticality and the crystalline order deteriorate with increasing temperature. At (a) 620, (b) 700, and (c) 750 °C, the morphology is ordered and vertical. At higher temperature (d) 800 (e) 820, and (f) 850 °C, the morphology exhibits disordered and less open structure. All the scale bars are 1 μm.

VOGN Formation and Growth. During the VOGN growth, the initial Volmer–Weber planar growth of two-dimensional graphitic islands on the Ni substrate ultimately impinge on each other, leaving a grain boundary region with numerous defects. Further deposition pushes the sp^2 bonds upward and dissociated species in the plasma then continuously provides the radicals, ions and neutrals to the vertically growing hexagonal lattice.[17,19] Figure 2a shows a schematic of the impinging planar graphite islands and the subsequent upturn in the growth dominated by sp^2 bonding, and the simultaneous dissolution of C atoms into the interstices of the Ni bulk. Figure 2b is an SEM of VOGN growth on a cylindrical Ni grid element which allows separation of the sheets. This provides a good, visual perspective of the vertical growth. High resolution transmission electron microscopy (TEM) image of the typical sheet edges grown at the temperature of 650 °C are shown in Figure 2c with the inset showing a selected area diffraction pattern of the nanosheet wall. The sheet thicknesses are greater than those previously observed from CH_4 feedstock (1–2 nm).[17] These fringes indicate 4 atomic layers with approximately the (002) spacing of graphite (0.335 nm). Some sheet edges are a bit smaller or a bit larger, but on average, about 5 graphene sheets.

Morphology of Vertically Oriented Graphene Nanosheets. The morphology of the VOGN on Ni substrates as a function of growth temperature is shown in Figure 3. From Figure 3, the surface morphology of VOGN can be grouped into two types. When the growth temperature was below 750 °C (Figure 3a–c), the morphology shows an ordered, uniform and very open structure with vertical growth. In general, this group is quite similar to that observed using CH_4 feedstock with the exceptions that the nanosheets produced using C_2H_2 are slightly thicker and more vertical.[17,20,21] At temperature above 800 °C (Figure 3d–f), there is a noticeable deterioration in the morphology. The sheets exhibit smaller size, irregular shape, disordered and more random morphology with much less openness to the substrate. When the temperature reached 850 °C, the structure consisted of smaller sheet pieces, much less ordered and "cauliflower-like". Compared to low temperature growth (Figure 3a–c), the growth in the high temperature range exhibited more exposed graphene planes and less open area.

The morphology comparisons by SEM with CH_4 growth showed very little obvious surface variation on the graphene side walls. Previous studies showed the height cross section for the C_2H_2–VOGN is much more uniform, vertical and the height variation is much smaller

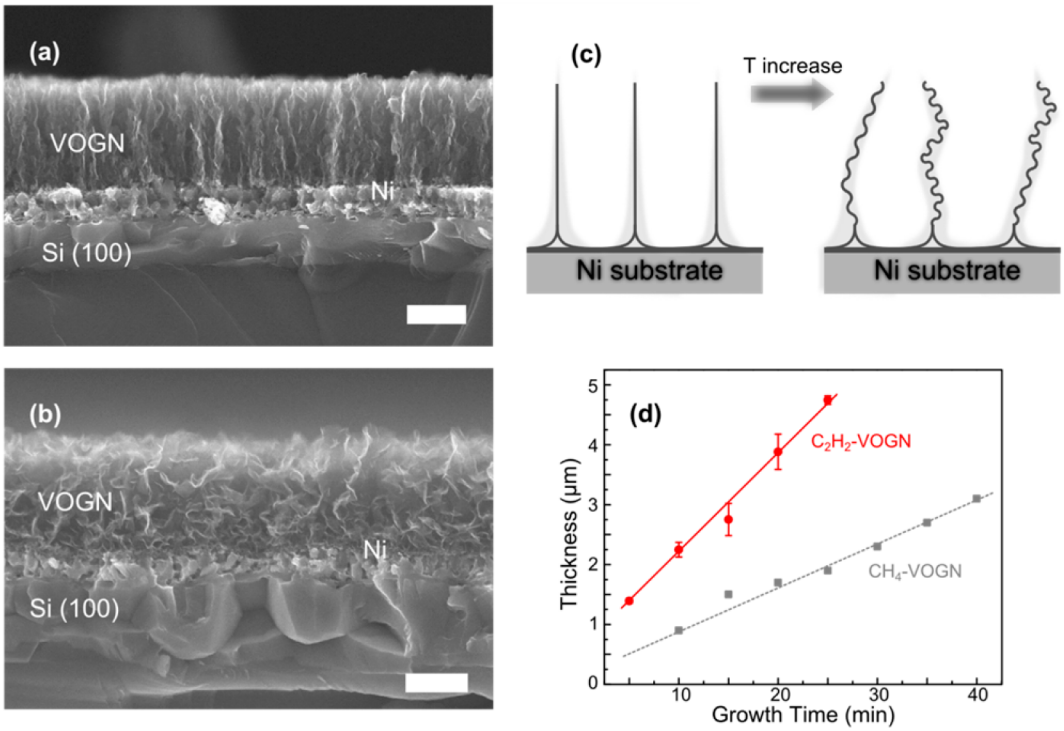

Figure 4. (a) A representative SEM image of the growth cross section of VOGN/Ni/Si(100) at 750 °C. (b) A representative image of the growth cross section of VOGN/Ni/Si(100) at 850 °C. (c) Schematics showing VOGN structural changes from an ordered, vertical morphology to a random, less vertical morphology when temperature increases. (d) The comparative plots of VOGN/Ni growth rates using C_2H_2 and CH_4 as feedstock.[17]

(<5%).[20] The reason for the more ordered shape may be the much smaller amount of hydrogen incorporated in the C_2H_2 growth. The feedstock partial pressure of H_2 is ~6 mTorr for the C_2H_2 growth and ~60 mTorr for the CH_4 growth. The relatively large amount of H incorporation in the hexagonal array during the CH_4–VOGN growth certainly would account for the thinner nanosheets and the declining nanosheet shape that occurs because of internal stresses as compared to the much more vertical C_2H_2 grown structures.

VOGN thin films using the same growth conditions were synthesized on Ni coated Si(100) substrates so that samples can be cleaved after deposition to expose the cross section. Figure 4a shows a representative SEM image of the cross section of a graphene film grown at 750 °C on Ni/Si(100), demonstrating ordered graphene perpendicular to the substrate. A typical cross section of films grown at the high temperature of 850 °C on Ni/Si(100) is shown in Figure 4b. Obviously, the verticality of sheets is substantially reduced. This structure change in the graphene sheets is shown schematically in Figure 4c. Combined with plan view morphology shown in Figure 3, the films grown at high temperature have less electrolyte access to the substrate, but expose more graphene molecular surface area.

The growth rate was estimated from the film thickness using the cross section of samples. Figure 4d shows the comparison of the growth rate between C_2H_2 feedstock and CH_4 feedstock. The growth rate measured for C_2H_2 feedstock was about 190 nm/min, in comparison to the growth rate of 70 nm/min for the CH_4 feedstock.[17] Thus, C_2H_2 feedstock produced 2.7 times faster growth. We attribute this to greater availability of carbon radicals, ions and neutrals in the C_2H_2 plasma, thus increasing the sp^2 bonding growth. The influence of temperature on the growth rate was also examined by measuring the thickness of films prepared at different temperatures. The results reveal all samples have comparable film thickness, indicating that temperature has negligible effect on the film thickness for the given growth time.

The physical adsorption isotherm of Ar on the VOGN/Ni sample (750 °C for 10 min) at 77.4 K is shown in Figure 5a. Figure 5b is the linearization of Figure 5a in accordance with the Brunauer–Emmett–Teller (BET) theory. Initially, both N_2 and Kr gases were tried, but did not provide sufficient sensitivity. The success of Ar suggests the smaller size of the atom allowed intercalation, and thus, a more measurable signal. Two thin film samples were tested. Excellent linear BET plots were obtained with a correlation coefficient of 0.998. Combining the intercept and the slope from this plot allowed a determination of the number of Ar atoms adsorbed in a monolayer. Multiplied by the area cross section of an argon atom (0.146 nm^2) gives the

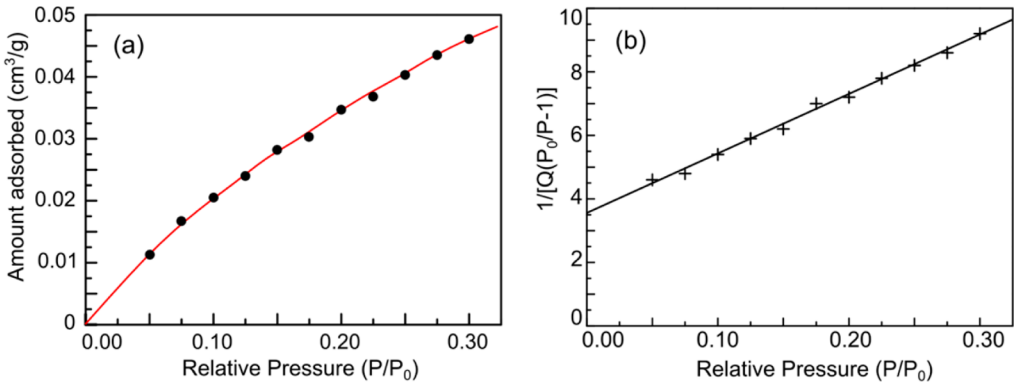

Figure 5. (a) Argon physical adsorption isotherm at 77.4 K of VOGN/Ni grown at 750 °C for 10 min. (b) The BET plot of (a). The ratio of the molecular surface area to the geometric area (footprint) was found to be ~310.

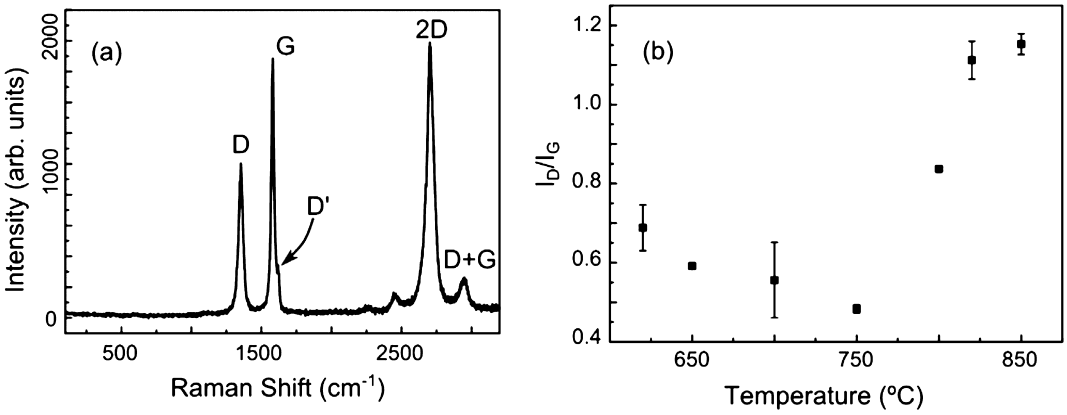

Figure 6. (a) A typical Raman spectrum of the VOGN films. (b) I_D/I_G ratio for the VOGN films as a function of temperature. Note the minimum at 750 °C which shows the lowest defect density.

molecular surface area. The ratios of molecular surface area to the geometric area (footprint area of the films) were determined, yielding an average value of 310. Using a model consisting of a square cross hatched array, 2 μm high with a 250 nm separation, to represent the VOGN films, then a mathematical estimate of the molecular surface area to geometric area gives a ratio of 64. Considering an average thickness of 5 graphene sheets per nanosheet, a ratio of 320 is obtained which is in reasonable agreement with the BET measurements.

Raman Spectrum of Vertically Oriented Graphene Nanosheets. The Raman spectrum of a typical VOGN is shown in Figure 6a. The characteristic D, G, and 2D peak at 1350, 1580, and 2680 cm^{-1} are as expected with a full width at half-maximum (fwhm) of ~40 cm^{-1} for the D band and ~20 cm^{-1} for the G band.[22−24] The intensity ratio of the D band (1350 cm^{-1}) to the G band (1580 cm^{-1}) is an indication of the amount of defects in carbon materials.[22,24] Over four spectra were collected at different spots on each sample, from which the average I_D/I_G ratio and the error bar of each VOGN film were calculated and shown in Figure 6b. At a temperature of 620 °C, the ratio is slightly less than 0.7 and continues to decrease to a minimum of ~0.45 at 750 °C, but then increases rapidly to ~1.15 at 850 °C. This is consistent with the morphology shown in Figure 3 and Figure 4. The results of a calculation of the corresponding nanosheets grain sizes by the empirical formula,[25] $(2.4 \times 10^{-10})\lambda_l^4(I_D/I_G)^{-1}$ (where λ_l is the wavelength of laser), ranged from 15 nm for the 850 °C growth to 35 nm for the 750 °C growth. The error bar of I_D/I_G ratio varies from sample to sample, which may be due to the inhomogeneous distribution of defects across samples.

The Raman I_D/I_G ratio can vary for both C_2H_2−VOGN and CH_4−VOGN, depending on the preparation conditions.[17,20] Specific conditions can be applied to both feedstock gases to achieve a ratio of less than 0.5. Further, when the CH_4−VOGN was degassed in high vacuum to 800 °C for 30 min, the ratio was observed to decrease to 0.25, suggesting some annealing of defects.[26] At lower temperatures of <750 °C, the surfaces are more open and allow the incident laser beam to sample more of the substrate which has more contribution from the amorphous growth. As the density of vertical sheets increases, the spectra reflect more of the more ordered vertical nanosheets. Eventually, at higher temperatures >750 °C, the vertical sheets deteriorate and dominate the defect contribution. With the use of Ar^+ ions at 1 kV to create vacancies in the existing CH_4−VOGN structures, it was found that

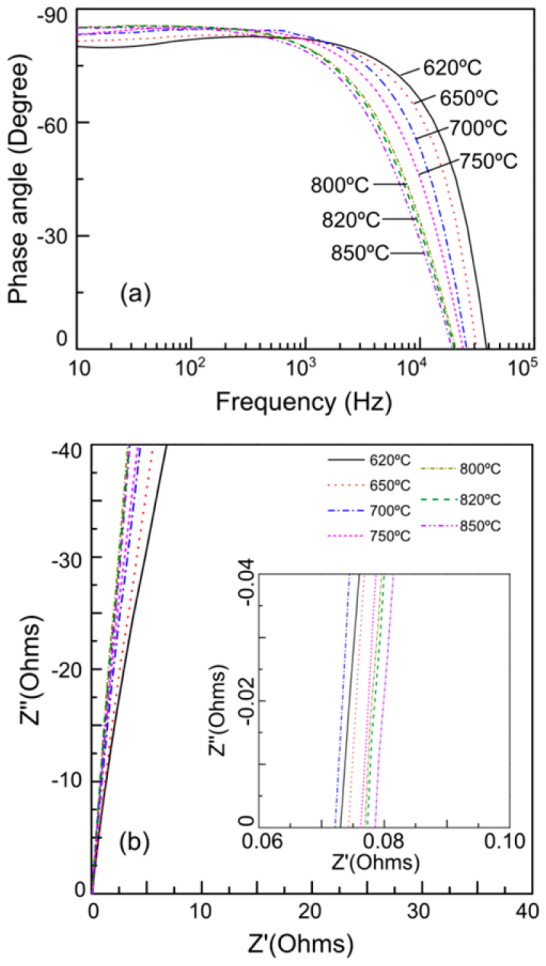

Figure 7. (a) Impedance phase angle as a function of frequency for the VOGN electrodes. The phase angle, θ, from 1 Hz up to 1 kHz is close to −90° for all samples. (b) Complex plane plot of the impedance for all growth temperatures. The inset shows the nearly vertical intersection of impedance and the real axis, showing absolutely no porous electrode behavior. The ESR of all samples is below 0.08 ohms.

both the I_D/I_G ratio and the fwhm photoelectron C 1s went up with increase in bombardment time (defects most likely vacancies) and the capacitance went up as well.[18] Similar work has been done on C_2H_2−VOGN with plasma etching. The same behavior was observed.[27]

Electrical Performance of VOGN-Electrode EDLCs. Symmetric, parallel electric double layer capacitors were fabricated using VOGN electrodes and characterized for electrical performance. The electrolyte was 25 wt % aqueous potassium hydroxide (KOH). Impedance measurements of capacitors fabricated with the VOGN electrodes are shown in Figure 7. The phase angle in Figure 7a approaches −90° and saturates at low frequency, showing the near-ideal capacitive behavior up to ∼1000 Hz for all VOGN samples at the given growth temperatures. The impedance phase angle of the capacitor made from C_2H_2 feedstock for lower growth temperatures of 620−750 °C reaches −45° at >10 kHz. The lowest temperature growth (620 °C) has the best response, which is consistent with the fact that the lower density VOGN has more free channels for movements of the electrolyte ions. The impedance phase angle at 120 Hz, important for ripple-current filtering applications, is approximately −85° and comparable to previously reported vertically oriented graphene EDLCs (−82° to −85°)[3,16,17] and commercially available aluminum electrolytic capacitors (−83°),[3] and significantly superior to the activated carbon EDLCs (∼0°)[6] and carbon nanotube EDLCs (−10° to −65°).[7−10] This high impedance phase angle also suggests the films are free of porous morphology which creates distributed charge storage that causes a transmission line electrical response. Figure 7b complex plane plots represent the impedance of EDLCs and shows nearly vertical lines that intersect the real axis at ∼90°, demonstrating that the EDLC has absolutely no porous electrode behavior. There are also no features associated with a series-passive layer. The insert plot shows the equivalent series resistances (ESR) are between 0.07 and 0.08 ohms, which are slightly higher than the 0.05 ohms observed with CH_4−VOGN/Ni, but still represent good ohmic connection between VOGN and Ni current collectors. This may be due to the higher resistance offered by the thicker nanosheets in this structure.

With the use of a series-RC circuit model, the specific capacitances of the EDLCs were calculated.[2,3,28] Figure 8a shows the capacitance variation over the frequency range up to 10^4 Hz for the temperature range investigated (capacitances at the frequency range higher than 10^4 Hz become divergent due to the artifact of the model). The specific capacitance increases as growth temperature increases over the entire frequency range. The capacitances at 120 Hz for all samples were compared in Figure 8b. The specific capacitance of VOGN EDLCs prepared using CH_4 as the feedstock was included for comparison. Compared to the CH_4−VOGN EDLCs, C_2H_2−VOGN provides significantly higher capacitance values. The roughly linear increase in specific capacitance with growth temperature corresponds to an increase in sheet surface area up to 750 °C where the defect density appears to be the best. Above this temperature, there appears to be a capacitance shift upward and then a linear continuation to an even higher surface area (above 800 °C) due to a change in the nanosheets morphology. A characteristic frequency, f_0, that corresponds to −45° impedance phase angle of the capacitor is commonly adopted to evaluate the frequency performance of cells. Since resistance and reactance have equal magnitudes at −45° impedance phase angle, f_0 defines the frontier between the capacitive and the resistive behavior of the cell.[3,29] The characteristic frequency f_0 of all EDLCs cells as a function of growth temperature were plotted in Figure 8b. The frequency f_0 goes down

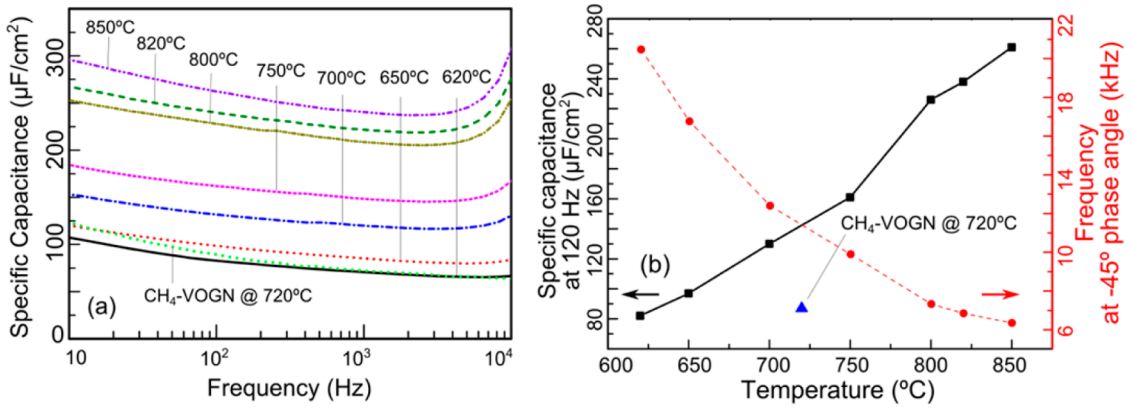

Figure 8. (a) Specific capacitance of EDLCs as a function of frequency. The higher the growth temperature, the higher the capacitance over the entire frequency range for all samples. (b) The specific capacitance of EDLCs at 120 Hz (black square blocks) for a 10 min growth and the characteristic frequency f_0 (red circular dots) as a function of growth temperature. The specific capacitance of VOGN EDLCs prepared using CH_4 as the feedstock at the temperature of 720 °C was included for comparison.[17]

as the temperature increases. This behavior is probably due to a loss of verticality in the sheets reducing the ion conductance between sheets and/or the loss in electronic conductivity due to an increase in defects.

DISCUSSION

Plasma. The RF-PECVD plasma is 80% C_2H_2 and 20% H_2 at a total pressure of ~20 mTorr. The inductively coupled plasma is created at an RF power of 1000 W. In a C_2H_2 plasma environment with and without the addition of He, Ar and Xe gases and the total pressures ranging from 0.1 to 0.7 Torr, H_2, C_4H_2 neutrals, $C_4H_2^+$, $C_4H_3^+$, and $C_2H_2^+$ were recorded as the dominant species.[30] Since the noble gases did not change the plasma chemistry significantly, we used only acetylene and hydrogen in this work. Another experiment using pure C_2H_2 plasma with a pressure of 30 mTorr under high power conditions showed that the plasma was dominated by C_4H_3 and C_2H radicals.[31] Creation of neutral plasma products, mainly $C_{2n}H_2$ polyacetylenes, is also reported.[32] These studies show that C_2H_2 plasma is dominated by species with an even number of carbon atoms such as radical C_4H_3 *etc.*[30−34] The possible production of reactive species at the surface of the graphene film as a result of atomic hydrogen induced erosion further complicates the system.[35] Therefore, it is extremely difficult to state with accuracy which species contributes most to the growth of the films. All the aforementioned ions, neutrals, and radicals could lead to the graphene formation.

Materials. As a substrate for EDLC electrode, Ni has several advantages. First, past research has shown that in a high vacuum environment, surface oxygen dissolves into the nickel bulk at elevated temperature, which then helps to make an intimate contact between graphene and Ni substrates without a passive oxide layer between the two.[36] Second, Ni possesses a relative high solubility for carbon as a solid solution. This is proved by the depth profile in Figure 1b which indicates that after nearly 12 h of Ar^+ ion sputtering (~1 μm deep) the carbon concentration has almost reached saturation with virtually no presence of oxygen component, thus suggesting a very good ohmic connection to the Ni. This intimate ohmic contact is further confirmed by the impedance complex plane in Figure 7b, which show no features associated with a series passive layer that would manifest itself as a high frequency semicircle. The high conductivity of the graphene sheets and the intimate ohmic contact between graphene and the Ni substrate establishes the low ESR values, which range from 0.07 to 0.08 ohms. Generally, the dominant resistance found in EDLCs with carbon electrodes has an ionic origin. The electronic resistances are usually small compared with ionic resistances and can be neglected. This is particularly true for VOGN electrodes where the VOGN is grown on and ohmically connected to the Ni current collector. Bulk electronic resistance of the VOGN/Ni therefore has negligible influence on the measured electrical performance. The ionic conductivity for 25 wt % aqueous KOH electrolyte normally is about 0.4 S/cm which is orders of magnitude smaller than that for the ohmic bonding of the carbon in nickel.

The growth of the VOGN using C_2H_2 feedstock resulted in an open structure that is important for eliminating porous electrode behavior and thus contributed to the high frequency response of devices. The lowest defect density in the sheets occurred at a growth temperature of 750 °C which gave a Raman I_D/I_G ratio ~0.45, but the data in Figure 7a show that it does not correspond to the best dynamic response, suggesting that the electron transport in the sheets was not the controlling issue of the dynamic response. Figure 7a shows that lower growth temperatures, with the more open structure and therefore better access to the electrolyte ions, give a higher frequency response, which suggests a higher efficiency for EDLCs used in filtering applications. Lower growth temperatures also

offer technological advantages that may allow the use of other substrates, like aluminum.

Capacitance. Figure 8b shows the specific capacitance at 120 Hz as a function of growth temperature for EDLCs made from C_2H_2 feedstock on Ni electrodes. The highest specific capacitance at 120 Hz was achieved for nanosheets growth at 850 °C, yielding a capacitance value of 265 μF/cm^2. The phase angle is still near −85° at 120 Hz, thus making it suitable for filtering applications. The capacitance values reported here are for a 10 min growth which yields nanosheets heights of about 2 μm. Sheng *et al.* reported thin film electrochemically reduced graphite oxide electrodes exhibited a specific capacitance of 283 μF/cm^2, but with 20 μm thick films (10 times thicker than the samples in this work).[15] Ren *et al.* deposited 2 μm-thick perpendicularly oriented graphene on a 200 μm Ni foam, producing a specific capacitance 360 μF/cm^2 at 120 Hz.[37] The usage of Ni foam is 100 times thicker, which substantially increases the graphene area per unit area of electrode footprint, thus, the areal specific capacitance. As the film height increases, the area of graphene sheets increases as well, but as shown in previous work using CH_4, a height increase of a factor of 4 produces only a 2-fold increase in capacitance.[17] Thus, assuming this analysis applies for VOGN grown from C_2H_2 feedstock, a VOGN film height of 16 μm (~80 min growth period) would provide a specific capacitance of 1 mF/cm^2.

Overall, the specific capacitance of the VOGN shows a linear increase with the growth temperature, presumably from a higher density of vertical sheets with its increased surface area. The VOGN morphology up to 750 °C (Figure 3) shows an increase in sheet density as well as more nanosheets waviness, which creates higher surface area. There is a notable step increase in the specific capacitance between 750 and 800 °C (Figure 8b). The morphology in this region shows dramatic change to a more disordered and rough structure compared to nanosheets grown at lower temperatures. A higher roughness factor causes higher surface area and, therefore, higher capacitance. Moreover, previous research showed that besides area, graphene defects can contribute to capacitance.[12,17,18,38] Hence, the increased defect density in the higher temperature samples also could lead to higher capacitance. It remains an interesting objective to determine the more significant contribution to increased capacitance, increased area or increased defect density. If defects were the dominant mechanism, it would seem that the parabolic shape of the Raman D band to G band ratio shown in Figure 6b would suggest a similar type of shape in Figure 8b, but the roughly linear shape suggests otherwise.

CONCLUSION

Creating an electric double layer capacitor with an electrical response similar to an electrolytic capacitor requires minimization of electronic and ionic resistances and elimination of distributed charge storage behavior. This work achieved these combined features using a unique electrode material: vertically oriented graphene. The highly conductive graphene sheets along with the low graphene/Ni substrate contact resistance minimize the electronic resistance. The vertically oriented, open geometry of the films facilitates electrolyte ion migration, contributing to low ionic resistance and eliminating the distribution of charges.

In this work, vertically oriented graphene nanosheets were prepared from C_2H_2 feedstock by RF-PECVD at temperature ranged from 620 to 850 °C. Higher temperatures produced a more dense and disordered morphology, which positively contributed to the capacitance value. All samples show the phase angle near −85° at 120 Hz, adequate for filtering applications and comparable to prevalent aluminum electrolytic capacitor technology. Compared to VOGN grown from CH_4 feedstock, the VOGN grown from C_2H_2 feedstock has shown significantly enhanced capacitance with a slight reduction in frequency response (but still sufficient for 120 Hz filtering). The VOGN/Ni growth rate from C_2H_2 feedstock is 2.7 times higher than the growth rate from CH_4 feedstock. The specific capacitance at 120 Hz of 265 μF/cm^2 was achieved for 850 °C growth temperature with a film height of only 2 μm (10 min growth), which provides promise of growing VOGN electrodes with a specific capacitance of greater than 1 mF/cm^2 EDLCs with sufficient AC filtering ability. This research has resulted in the growth of a small mass and volume electrical double layer capacitor with the ultrafast frequency response, providing promise to substantially lower the mass and volume of present filtering electronics.

METHODS

Growth of Vertically Oriented Graphene. Nickel substrates (75 μm thick, 1.9 cm diameter) were ultrasonically cleaned sequentially in acetone and ethanol, and blown dry with moisture-free air and then positioned in the vacuum chamber on an Al_2O_3 platen encapsulating rhenium−tungsten wire (3%Re−97%W, diameter 0.34 mm) resistive heater. A two-hole, flat, polished tantalum mask was placed concentrically on top of the substrates to define the graphene growth region (1.27 cm diameter) for a pair of symmetric electrodes. The flatness of the mask was absolutely necessary to ensure uniform heating of the Ni foils. Details of the experimental system and the RF-PECVD vacuum system have been previously reported.[16,17,21] In brief, the sequence of steps begins by evacuating the system to a pressure <2 mTorr. Upon reaching steady state pressure, hydrogen was admitted. The Ni substrates were heated in 60 mTorr of hydrogen to a desired growth temperature. Argon was then admitted into the chamber to produce a combined pressure of ~100 mTorr. The heated substrates were plasma-etched for

5 min to further remove surface contamination. Nanosheet growths were conducted using 80% C_2H_2 and 20% H_2 at a total pressure of ~20 mTorr and 1000 W plasma power for 10 min. During growth, the Ta mask and the substrates were unbiased and allowed to electrically float to near the plasma potential.

To obtain the height information, VOGN thin films were also synthesized on 500 nm Ni coated Si(100) substrates using the same growth conditions. The samples were cleaved after deposition to expose the cross section and thus allow height measurement. Growth times from 5 to 25 min were performed to investigate the vertical growth rates.

Characterizations. The surface morphology of the VOGN was examined using scanning electron microscopy (SEM, Hitachi S-4700, operated at 15 kV). Cross sections of samples grown on Ni/Si substrates were also measured with SEM to determine the thickness and thus growth rate of the VOGN. The structure and defect information on the graphene films were studied by a Renishaw in-Via Raman spectroscope using a 514 nm wavelength laser. The individual sheets were examined by transmission electron microscopy (TEM, JEOL JEM 2010F, 200 keV)) to assess the sheet thickness and crystalline order. The argon adsorption experiments were conducted at 77.4 K by Particle Technology Laboratories (Downers Grove, IL). The specific surface area of VOGN/Ni samples were calculated from the Brunauer–Emmett–Teller (BET) plots of the adsorption isotherms.

The surfaces of the substrates before and after coating were examined by Auger electron spectroscopy (AES, Physical Electronics 590 system with a 15–255 GAR double pass cylindrical mirror analyzer operated at 2 kV beam energy and 0.5 μA beam current). For surfaces before coating, the Ni substrates were initially degreased in an ultrasonic cleaner, sequentially with acetone for 10 min followed by 10 min in ethyl alcohol and then dried using ultrahigh purity nitrogen. The substrates were then admitted to the introduction chamber ($p < 1 \times 10^{-9}$ Torr) and radiative heated to 250 °C for 30 min to degas the adsorbed water on the sample holder and then transferred to the analysis chamber ($p < 1 \times 10^{-11}$ Torr) for surface study. Samples after coating were directly admitted to the introduction chamber, degassed, allowed to sit for 24 h and then transferred to the analysis chamber. AES depth profiles, after VOGN growth, were conducted using 5 kV Ar^+ ions, 1 μA/cm^2 beam current density, to determine the extent of carbon diffusion into the Ni substrate.

Cell Unit Assembly and Capacitance Measurements. Symmetric electric double layer capacitors were fabricated using VOGN electrodes and characterized for electrical performance. The EDLC used two identical 1.9 cm-diameter, 75 μm-thick Ni disks with nanosheets growth over the central 1.27 cm-diameter region (1.26 cm^2). The two disks were separated by a 25-μm-thick microporous polypropylene separator that had 48% open area (Polypore International, Inc., Charlotte, NC). The VOGN and separator were wetted with an aqueous electrolyte (25 wt % potassium hydroxide) before sealing the perimeter of the disks with a thermoplastic using an impulse heat-seal apparatus. These packaged prototypes were 1.9 cm diameter by ~175 μm thick and had a mass of less than 1 g. The height of the VOGN on each electrode was about 2 μm, which is negligible compared with device dimensions. A nickel lead was spot-welded to the backside of each Ni substrate to make electrical connection. This EDLC design circumvents the passive-layer problem often encountered with the usual button/coin cells designs.

Electrochemical impedance spectroscopy (EIS) measurements were performed at 0.5 V bias after electrodes were completely wetted by the electrolyte. The AC capacitance was derived, assuming a series-RC circuit model, from $C = (-1/2\pi f z'')$, where f is frequency (in Hz) and z'' is the corresponding imaginary part of the impedance. The specific capacitance was calculated by $C_S = C/A$, where C is the AC capacitance of the device and A is the geometric area (footprint area) of the VOGN growth region. All values reported are for two-terminal devices, not single electrodes.

Conflict of Interest: The authors declare no competing financial interest.

Acknowledgment. The authors wish to acknowledge the Army Research Laboratory (ARL) for financial support (ARL W911QX-13-C-0056) and thank Dr. Matt Ervin of the ARL for many helpful discussions. R. A. Quinlan would like to acknowledge financial support by the Carderock Division of the Naval Surface Warfare Center's In-house Laboratory Independent Research Program administrated under ONR's Program Element 0601152N.

REFERENCES AND NOTES

1. Miller, J. R.; Burke, A. F. Electrochemical Capacitors: Challenges and Opportunities for Real-World Applications. *Electrochem. Soc. Interface* **2008**, *17*, 53–55.
2. Conway, B. E. In *Electrochemical Supercapacitors: Scientific Fundamentals and Technological Applications*; Kluwer Academic/Plenum Publishers: New York, 1999.
3. Miller, J. R.; Outlaw, R. A.; Holloway, B. C. Graphene Double-Layer Capacitor with AC Line-Filtering Performance. *Science* **2010**, *329*, 1637–1639.
4. Simon, P.; Gogotsi, Y. Materials for Electrochemical Capacitors. *Nat. Mater.* **2008**, *7*, 845–854.
5. Frackowiak, E.; Béguin, F. Carbon Materials for the Electrochemical Storage of Energy in Capacitors. *Carbon* **2001**, *39*, 937–950.
6. Pandolfo, G.; Hollenkamp, A. F. Carbon Properties and Their Role in Supercapacitors. *J. Power Sources* **2006**, *157*, 11–27.
7. Niu, C.; Sichel, E. K.; Hoch, R.; Moy, D.; Tennent, H. High Power Electrochemical Capacitors based on Carbon Nanotube Electrodes. *Appl. Phys. Lett.* **1997**, *70*, 1480–1482.
8. Du, C.; Pan, N. Supercapacitors using Carbon Nanotubes Films by Electrophoretic Deposition. *J. Power Sources* **2006**, *160*, 1487–1494.
9. Basiricò, L.; Lanzara, G. Moving towards High-Power, High-Frequency and Low-Resistance CNT Supercapacitors by Tuning the CNT Length, Axial Deformation and Contact Resistance. *Nanotechnology* **2012**, *23*, 305401.
10. Honda, Y.; Haramoto, T.; Takeshige, M.; Shiozaki, H.; Kitamura, T.; Ishikawa, M. Aligned MWCNT Sheet Electrodes Prepared by Transfer Methodology Providing High-Power Capacitor Performance. *Electrochem. Solid-State Lett.* **2007**, *110*, A106–110.
11. Stoller, M. D.; Park, S.; Zhu, Y.; An, J.; Ruoff, R. S. Graphene-Based Ultracapacitors. *Nano Lett.* **2008**, *8*, 3498–3502.
12. Zhu, Y.; Murali, S.; Stoller, M. D.; Ganesh, K. J.; Cai, W.; Ferreira, P. J.; Pirkle, A.; Wallace, R. M.; Cychosz, K. A.; Thommes, M.; *et al.* Carbon-based Supercapacitors Produced by Activation of Graphene. *Science* **2011**, *332*, 1537–1541.
13. Wang, Y.; Shi, Z.; Huang, Y.; Ma, Y.; Wang, C.; Chen, M.; Chen, Y. Supercapacitor Devices Based on Graphene Materials. *J. Phys. Chem. C* **2009**, *113*, 13103–13107.
14. Zhang, L. L.; Zhao, X. S. Carbon-Based Materials as Supercapacitor Electrodes. *Chem. Soc. Rev.* **2009**, *38*, 2520–2531.
15. Sheng, K.; Sun, Y.; Li, C.; Yuan, W.; Shi, G. Ultrahigh-Rate Supercapacitors Based on Eletrochemically Reduced Graphene Oxide for AC Line-Filtering. *Sci. Rep.* **2012**, *2*, 247.
16. Miller, J. R.; Outlaw, R. A.; Holloway, B. C. Graphene Electric Double Layer Capacitor with Ultra-High-Power Performance. *Electrochim. Acta* **2011**, *56*, 10443–10449.
17. Cai, M.; Outlaw, R. A.; Butler, S. M.; Miller, J. R. A High Density Of Vertically-oriented Graphenes for Use in Electric Double Layer Capacitors. *Carbon* **2012**, *50*, 5481–5488.
18. Quinlan, R. A.; Cai, M.; Outlaw, R. A.; Butler, S. M.; Miller, J. R.; Mansour, A. N. Investigation of Defects Generated in Vertically Oriented Graphene. *Carbon* **2013**, *64*, 92–100.
19. Zhu, M.; Wang, J.; Holloway, B. C.; Outlaw, R. A.; Zhao, X.; Hou, K.; Shutthanandan, V.; Manos, D. M. A Mechanism for Carbon Nanosheet Formation. *Carbon* **2007**, *45*, 2229–2234.
20. Zhu, M. Y.; Outlaw, R. A.; Bagge-Hansen, M.; Chen, H. J.; Manos, D. M. Enhanced Field Emission of Vertically Oriented Carbon Nanosheets Synthesized by C_2H_2/H_2 Plasma Enhanced CVD. *Carbon* **2011**, *49*, 2526–2531.

21. Wang, J.; Zhu, M.; Outlaw, R. A.; Zhao, X.; Manos, D. M.; Holloway, B. C. Synthesis of Carbon Nanosheets by Inductively Coupled Radio-frequency Plasma Enhanced Chemical Vapor Deposition. *Carbon* **2004**, *42*, 2867–2872.
22. Ferrari, A. C.; Robertson, J. Interpretation of Raman Spectra of Disordered and Amorphous Carbon. *Phys. Rev. B* **2000**, *61*, 14095–14107.
23. Ferrari, A. C.; Meyer, J. C.; Scardaci, V.; Casiraghi, C.; Lazzeri, M.; Mauri, F.; Piscanec, S.; Jiang, D.; Novoselov, K. S.; Roth, S.; *et al.* Raman Spectrum of Graphene and Graphene Layers. *Phys. Rev. Lett.* **2006**, *97*, 187401.
24. Pimenta, M. A.; Dresselhaus, G.; Dresselhaus, M. S.; Cançado, L. G.; Jorio, A.; Saito, R. Studying Disorder in Graphite–based Systems by Raman Spectroscopy. *Phys. Chem. Chem. Phys.* **2007**, *9*, 1276–1290.
25. Cançado, L. G.; Takai, K.; Enoki, T.; Endo, M.; Kim, Y. A.; Mizusaki, H.; Jorio, A.; Coelho, L. N.; Magalhaes-Paniago, R.; Pimenta, M. A. General Equation for the Determination of the Crystallite Size La of Nanographite by Raman Spectroscopy. *Appl. Phys. Lett.* **2006**, *88*, 163106.
26. Zhao, X.; Outlaw, R. A.; Wang, J. J.; Zhu, M. Y.; Smith, G. D.; Holloway, B. C. Thermal Desorption of Hydrogen from Carbon Nanosheets. *J. Chem. Phys.* **2006**, *124*, 194704.
27. This work is presently being prepared for publication.
28. Kötz, R.; Carlen, M. Principles and Applications of Electrochemical Capacitors. *Electrochim. Acta* **2000**, *45*, 2483–2498.
29. Taberna, P. L.; Simon, P.; Fauvarque, J. F. Electrochemical Characteristics and Impedance Spectroscopy Studies of Carbon-Carbon Supercapacitors. *J. Electrochem. Soc.* **2003**, *150*, A292–A300.
30. Vasile, M. J.; Smolinsky, G. The Chemistry of Radio Frequency Discharges: Acetylene and Mixtures of Acetylene with Helium, Argon and Xenon. *Int. J. Mass Spectrom. Ion. Phys.* **1977**, *24*, 11–23.
31. Doyle, J. R. Chemical Kinetics in Low Pressure Acetylene Radio Frequency Glow Discharges. *J. Appl. Phys.* **1997**, *82*, 4763–4771.
32. Benedikt, J. Plasma-Chemical Reactions: Low Pressure Acetylene Plasmas. *J. Phys. D.: Appl. Phys.* **2010**, *43*, 043001.
33. Deschenaux, C.; Affolter, A.; Magni, D.; Hollenstein, C.; Fayet, P. Investigations of CH_4, C_2H_2 and C_2H_4 Dusty RF Plasmas by Means of FTIR Absorption Spectroscopy and Mass Spectrometry. *J. Phys. D.:Appl. Phys.* **1999**, *32*, 1876.
34. Consoli, A.; Benedikt, J.; von Keudell, A. Initial Polymerization Reactions in Particle-Forming Ar/He/C_2H_2 Plasmas Studied *via* Quantitative Mass Spectrometry. *J. Phys. Chem. A* **2008**, *112*, 11319–11329.
35. Bagge-Hansen, M.; Outlaw, R. A.; Zhu, M. Y.; Chen, H. J.; Manos, D. M. Hyperthermal Atomic Hydrogen and Oxygen Etching of Vertically Oriented Graphene Sheets. *J. Vac. Sci. Technol. B* **2009**, *27*, 2413–2419.
36. Holloway, P. H.; Outlaw, R. A. The Effects of Temperature upon NiO Formation and Oxygen Removal on Ni (110). *Surf. Sci.* **1981**, *111*, 300–316.
37. Ren, G.; Pan, X.; Bayne, S.; Fan, Z. Kilohertz Ultrafast Electrochemical Supercapacitors Based on Perpendicularly-oriented Graphene Grown inside of Nickel Foam. *Carbon* **2014**, *71*, 94–101.
38. Kim, T.; Lim, S.; Kwon, K.; Hong, S. H.; Qiao, W.; Rhee, C. K.; Yoon, S. H.; Mochida, I. Electrochemical Capacitances of Well-Defined Carbon Surfaces. *Langmuir* **2006**, *22*, 9086–9088.